Cite as: W. Yin *et al.*, *Science* 10.1126/science.abn8863 (2022).

Structures of the Omicron Spike trimer with ACE2 and an anti-Omicron antibody

Wanchao Yin[1]†*, Youwei Xu[1]†, Peiyu Xu[1]†, Xiaodan Cao[2]†, Canrong Wu[1]†, Chunyin Gu[2]†, Xinheng He[1,3], Xiaoxi Wang[1], Sijie Huang[1], Qingning Yuan[4], Kai Wu[4], Wen Hu[4], Zifu Huang[5], Jia Liu[2], Zongda Wang[2], Fangfang Jia[2], Kaiwen Xia[2], Peipei Liu[2], Xueping Wang[2], Bin Song[6], Jie Zheng[6], Hualiang Jiang[3,5,7], Xi Cheng[3,5], Yi Jiang[1,3,5], Su-Jun Deng[2]*, H. Eric Xu[1,3,7]*

[1]The CAS Key Laboratory of Receptor Research, Shanghai Institute of Materia Medica, Chinese Academy of Sciences, Shanghai 201203, China. [2]Shanghai Jemincare Pharmaceuticals Co., Ltd., Shanghai 201203, China. [3]University of Chinese Academy of Sciences, Beijing 100049, China. [4]The Shanghai Advanced Electron Microscope Center, Shanghai Institute of Materia Medica, Chinese Academy of Sciences, Shanghai 201203, China. [5]State Key Laboratory of Drug Research, Shanghai Institute of Materia Medica, Chinese Academy of Sciences, Shanghai 201203, China. [6]Immunological Disease Research Center, Shanghai Institute of Materia Medica, Chinese Academy of Sciences, .Shanghai 201203, China. [7]School of Life Science and Technology, ShanghaiTech University, 201210 Shanghai, China.

†These authors contributed equally to this work.

*Corresponding author. Email: wcyin@simm.ac.cn (W.Y.); dengsujun@jemincare.com (S.-J.D.); eric.xu@simm.ac.cn (H.E.X.)

The severe acute respiratory syndrome coronavirus 2 (SARS-CoV-2) Omicron variant has become the dominant infective strain. We report the structures of the Omicron spike trimer on its own or in complex with ACE2 or an anti-Omicron antibody. Most Omicron mutations are located on the surface of the spike protein, which change binding epitopes to many current antibodies. In the ACE2 binding site, compensating mutations strengthen RBD binding to ACE2. Both the RBD and the apo form of the Omicron spike trimer are thermodynamically unstable. An unusual RBD-RBD interaction in the ACE2-spike complex supports the open conformation and further reinforces ACE2 binding to the spike trimer. A broad-spectrum therapeutic antibody, JMB2002, which has completed a Phase 1 clinical trial, maintains neutralizing activity against Omicron. JMB2002 binds to RBD differently from other characterized antibodies and inhibits ACE2 binding.

The Omicron variant of severe acute respiratory syndrome coronavirus 2 (SARS-CoV-2), the causative virus of COVID-19, was initially reported from South Africa in November 2021, and quickly became the dominant strain worldwide (*1*). Phylogenetic tree analyses reveal that Omicron evolved independently from previous variants of concerns (VOC), including the predominant Alpha, Beta, Gamma, and Delta variants (Fig. 1A) (*2*–*5*). Compared to the original wildtype (WT) strain of SARS-CoV-2, Omicron has 60 amino acid mutations, of which 37 mutations are in the spike protein, the target of most COVID-19 vaccines and therapeutic antibodies (Fig. 1B). This high variation is reflected in different behavior with the Omicron variant showing enhanced transmission, antibody evasion, and vaccine resistance (*6*–*8*).

To study the mechanism for Omicron's enhanced transmission, we first biochemically characterized the interactions of the SARS-CoV-2 receptor ACE2 with the trimer of the spike extracellular domain (ECD) from Omicron and the original WT strain, both of which contain proline substitutions (2P or 6P) and a mutated furin cleavage site to stabilize the prefusion conformation (*9*, *10*). Monomeric human ACE2 bound to immobilized Omicron trimeric spike protein with approximately 6-fold higher affinity (K_D=2.5 ± 0.6 nM) than WT spike trimer (K_D=14.7 ± 4.9 nM). The dimeric human ACE2 bound to immobilized biotinylated Omicron spike trimer (K_D=0.3 ± 0.2 nM) with approximately 9-fold higher avidity than WT (K_D=2.7 ± 1.4 nM) (Fig. 1, C and D). We then studied the interactions of ACE2 with monomeric receptor binding domain (RBD) from Omicron and WT strains. Monomeric human ACE2 bound to immobilized Omicron RBD (K_D=38.9 ± 10.5 nM) with approximately 2-fold higher affinity than WT RBD (K_D=75.5 ± 2.1 nM) (Fig. 1, C and D). The enhanced interaction of Omicron spike and RBD proteins with human ACE2 is consistent with previously published data (*11*), and may contribute to the increased infectivity of the Omicron variant.

To determine the structural basis of higher affinity of the Omicron spike trimer for ACE2, we solved the structure of the ACE2-Omicron spike trimer complex at a global resolution of 2.77 Å (table S1). Despite an excess of ACE2 (molar ratio of 3.2 ACE2 to 1 spike trimer; fig. S1A), we only observed strong density for one ACE2 bound to one RBD from the spike trimer in the open "up" conformation (Fig. 2A and fig. S2). The other two RBDs, with clear density, are in the closed "down" conformation. Particle classification revealed that the majority of picked particles (~70%) do not have ACE2 bound. We also determined the structure of this apo Omicron spike trimer at a global resolution of 2.56 Å (fig. S2 and table S1). All three RBDs are in the closed down conformation but they are less visible in the high-resolution map (2.56 Å; fig. S3A),

yet become more visible in lower resolution maps (4.5 Å and 6.5 Å; fig. S3, B and C). This contrasts with the clear visibility of the three RBDs in the ACE2-Omicron spike complex in a high-resolution map (2.56 Å; Fig. 2A), indicating that the RBD in the apo form is more dynamic and ACE2 binding likely stabilizes the conformation of the three RBDs. Thermal shift assays at pH7.4 revealed that the Omicron and WT RBD have single melting temperatures of 45.7°C and 51.0°C respectively (fig. S1C), indicating that the Omicron RBD is less stable than the WT RBD. In contrast, both the Omicron and WT spike trimer displayed two melting temperatures (fig. S1D), with the high Tm corresponding to the dissociation of the spike trimer and the low Tm corresponding to unfolding of the RBD. The melting temperature profile of WT spike trimer is similar to previous reports (*10*, *12*). Tm1 of both Omicron and WT spike trimer is similar to the respective Tm for the isolated RBD (fig. S1, C and D), indicating that the Omicron RBD within the context of the spike trimer remains less stable than the WT RBD. We further confirmed the highly flexible nature of the Omicron RBD by performing hydrogen-deuterium exchange mass spectrometry (HDX), which showed that the Omicron spike trimer has an overall higher rate of HDX (fig. S4), particularly in the RBD region, consistent with its lower thermal stability.

Mapping the 37 mutations onto the up protomer of the ACE2 bound spike trimer reveals that most mutations are located on the surface of the spike protein, with many of them in known epitopes of therapeutic antibodies (Fig. 2B). We grouped the surface mutations into 3 hotspots (Fig. 2C and table S2). Eight mutations in the NTD (hotspot I) would affect the structures of the epitopes for a number of antibodies, for example, Δ143-145 would remove the epitope for the 4A8 antibody (*13*). 15 mutations are in the RBD, which contains the ACE2 binding site as well as the epitopes for 90% of antibodies induced by infection or vaccination. 10 of these mutations are in the RBM (hotspot II) and 5 are near the core structure domain (hotspot III) (Fig. 2C). Hot spot II encompasses the epitopes for therapeutic antibodies, AZD1061, REGN10987 and REGN10933 and hotspot III overlaps the epitope for LY-CoV555 (Fig. 2B) (*14–16*).

Local refinement of the ACE2-RBD region produced a high-quality map at 2.57 Å resolution, which allowed unambiguous building of the ACE2-RBD complex (Fig. 3A, table S1, and fig. S2). Though their RBDs differ at 15 residues, the overall structure of the Omicron ACE2-RBD complex is similar to two high resolution X-ray structures of the WT ACE2-RBD complex (PDB codes: 6LZG and 6M0J (*17*, *18*)), with the Cα atoms of the whole RBD deviating by less than 0.4 Å (Fig. 3B and table S3). We do see local differences at the ACE2-RBD interface; the Omicron RBD forms extra interactions with ACE2, including interactions from RBD mutations S477N, Q493R, Q496S, Q498R, and N501Y to ACE2 (Fig. 3C). In particular, the side chain of S477N forms two extra hydrogen bonds with S19 of ACE2; the Q498R mutation forms two additional hydrogen bonds with Q42 and D38 from ACE2; and the N501Y mutation forms extensive packing interactions with ACE2 residues Y41 and K353. These additional interactions may compensate for the loss of polar interactions between WT RBD and ACE2 caused by RBD mutations K417N and E484A (Fig. 3, C and D), consistent with the enhanced affinity of the Omicron RBD with ACE2 (Fig. 1, C and D).

We observe RBD-RBD interactions from one of the two down RBDs to the up RBD (Fig. 3A), with the interface comprised by residues A475 and F486 from the down RBD and residues L368, F374 and T385 from the up RBD (Fig. 3A and fig. S5A). Structure comparison reveals that the RBD-RBD interface is not observed within the WT spike trimer because of movement of a loop (residues 368-374), caused by Omicron RBD mutations S371L, S373P, G339D, and S375F, which are in hotspot III (Fig. 2C and fig. S5A). This RBD-RBD interaction may stabilize the up conformation of the RBD that promotes ACE2 binding. In addition, the Omicron mutations S371L, S373P and S375F are located at the entrance to the fatty acid binding pocket in the WT RBD (*19*), and these Omicron mutations distort the fatty acid binding pocket (fig. S5B), thus destabilizing the RBDs in the all closed-down conformation. Consistent with involvement of spike dynamics, ACE2 binds to the Omicron spike trimer with 6-9 fold higher avidity than to the WT spike trimer, but binds to the Omicron RBD monomer with 2- fold higher affinity than to WT RBD. (Fig. 1, C and D). We suggest that in addition to destabilization of RBDs in the closed conformation, the RBD-RBD interactions that stabilize one RBD in the open up conformation within the spike trimer, may act together with the compensating mutations in the ACE2 binding site to contribute to the higher affinity of Omicron and this likely plays a role in its higher infectivity.

We had previously discovered an antibody, JMB2002, which showed potent efficacy against the WT SARS-CoV-2 in cell-based models as well as in a rhesus monkey model (*20*). JMB2002 has completed Phase I clinical trial in healthy donors with excellent safety and pharmacokinetic properties and has been approved for a clinical trial in the USA (IND 154745). We evaluated the binding of JMB2002 to WT and Omicron spike trimers. JMB2002 Fab bound the Omicron spike trimer with ~4-fold increased affinity (K_D=3.2 ± 3.0 nM) compared to WT spike trimer (K_D=12.2 ± 11.6 nM), while JMB2002 IgG showed similar avidity for Omicron spike trimer (K_D=0.4 ± 0.1 nM) and WT (K_D=0.5 ± 0.3 nM) (Fig. 4, A to D). Furthermore, JMB2002 was able to directly inhibit the binding of ACE2 to the Omicron spike trimer with an IC_{50} of 1.8 nM (Fig. 4E). In pseudovirus neutralization assays, JMB2002 effectively blocked the entry of Omicron pseudovirus into human ACE2 expressing cells in addition to its

blocking of the WT pseudovirus (Fig. 4F and fig. S6A). JMB2002 was also able to neutralize a number of VOCs, including variants of Alpha, Beta, and Gamma, but not Delta (fig. S6, B to E).

To reveal the basis of JMB2002 inhibition of Omicron, we solved the structure of the Omicron spike trimer bound to a Fab from JMB2002 at a global resolution of 2.69 Å (Fig. 5A, table S1, and figs. S7 and S8). To stabilize the constant regions of Fab, we used a nanobody that binds to the interface between the variable and constant regions of the light chain (*21*). The EM density map reveals the binding of 2 Fab molecules to two RBDs (one up and one down) of the trimeric spike (Fig. 5, A and B). The overall structure of the spike trimer in the Fab-bound complex is very similar to that of the ACE2-bound complex, with an RMSD of 1.0 Å over all Cα atoms of the spike trimer, including the unusual RBD-RBD dimer configuration (fig. S9, A and B).

Within the Fab-spike trimer structure, both Fabs bind to the same region in their respective RBD (Fig. 5, C and D). Local refinement of the Fab bound RBD structure generated a density map to a resolution of 2.47 Å (figs. S7G and S8D), which provides detailed interactions between Fab and RBD. The Fab binding site does not overlap with the ACE2 binding site (fig. S9C). However, in the context of the trimer, Fab binding to the down RBD would clash with ACE2 binding to the up RBD (Fig. 5E), consistent with direct inhibition of ACE2 binding to the Omicron spike trimer by JMB2002 (Fig. 4E).

Particle classification also revealed two additional antibody-bound complexes at a global resolution of 2.92 Å and 3.18 Å, respectively (figs. S7 and S8). One of the two complexes has the spike trimer with one-up RBD bound to one Fab and two-down RBDs in the apo state (fig. S8A). The other complex contains the spike trimer with two-up RBDs and one down RBD, with each RBD bound to one Fab (fig. S8C). The up-down RBD-RBD interactions within the spike trimer are conserved in these complexes. The diverse configuration and stoichiometry ratio of the spike trimer bound to the antibody further highlight the conformation flexibility of the Omicron spike RBD. The ability of the spike trimer to bind to three Fab molecules provides additional basis for the potency of JMB2002 against Omicron.

The L452R mutation in the Delta variant is at the center of the binding epitope of JMB2002 and this mutation would clash with Y102 from the heavy chain of the Fab (Fig. 5F), thus providing an explanation for its loss of potency against the Delta variant. In addition, the binding site of the JMB2002 Fab on the RBD is distinct from the epitopes for previously defined class I to class IV antibodies (Fig. 5G) (*22*), thus JMB2002 represents a new class of antibody against the spike trimer.

In this paper, we report biochemical characterization of the Omicron spike trimer and its binding to ACE2. Our data reveal that the Omicron RBD is less stable and more dynamic than the WT RBD, and the Omicron spike trimer has 6-9 fold increased affinity for binding to ACE2. We further solved the structures of the Omicron spike trimer in the apo state, or bound to ACE2 or an anti-Omicron antibody. The ACE2 bound structure reveals that the Omicron spike trimer contains an unusual RBD-RBD interaction and extra interactions in the ACE2-RBD interface, both of which contribute to the higher affinity of ACE2 to the Omicron spike trimer. Structural analysis of the Omicron spike trimer also provides a mechanistic basis for the ability of Omicron to escape most therapeutic antibodies and reduce the efficacy of vaccinations.

In addition, our structures of antibody-bound Omicron spiker trimer uncover a distinct mode of antibody binding to the spike trimer, in which the unusual RBD-RBD configuration is preserved. The binding epitope of this broad-spectrum antibody is different from previous anti-SARS-CoV-2 antibodies, therefore opening a new venue for antibody drug discovery targeting various strains of SARS-CoV-2, including Omicron.

REFERENCES AND NOTES

1. J. Ai, H. Zhang, Y. Zhang, K. Lin, Y. Zhang, J. Wu, Y. Wan, Y. Huang, J. Song, Z. Fu, H. Wang, J. Guo, N. Jiang, M. Fan, Y. Zhou, Y. Zhao, Q. Zhang, Q. Liu, J. Lv, P. Li, C. Qiu, W. Zhang, Omicron variant showed lower neutralizing sensitivity than other SARS-CoV-2 variants to immune sera elicited by vaccines after boost. *Emerg. Microbes Infect.* **11**, 337–343 (2022). Medline
2. M. Yuan, D. Huang, C. D. Lee, N. C. Wu, A. M. Jackson, X. Zhu, H. Liu, L. Peng, M. J. van Gils, R. W. Sanders, D. R. Burton, S. M. Reincke, H. Prüss, J. Kreye, D. Nemazee, A. B. Ward, I. A. Wilson, Structural and functional ramifications of antigenic drift in recent SARS-CoV-2 variants. *Science* **373**, 818–823 (2021). doi:10.1126/science.abh1139 Medline
3. Y. Cai, J. Zhang, T. Xiao, C. L. Lavine, S. Rawson, H. Peng, H. Zhu, K. Anand, P. Tong, A. Gautam, S. Lu, S. M. Sterling, R. M. Walsh Jr., S. Rits-Volloch, J. Lu, D. R. Wesemann, W. Yang, M. S. Seaman, B. Chen, Structural basis for enhanced infectivity and immune evasion of SARS-CoV-2 variants. *Science* **373**, 642–648 (2021). doi:10.1126/science.abi9745 Medline
4. R. Earnest, R. Uddin, N. Matluk, N. Renzette, K. J. Siddle, C. Loreth, G. Adams, C. H. Tomkins-Tinch, M. E. Petrone, J. E. Rothman, M. I. Breban, R. T. Koch, K. Billig, J. R. Fauver, C. B. F. Vogels, S. Turbett, K. Bilguvar, B. De Kumar, M. L. Landry, D. R. Peaper, K. Kelly, G. Omerza, H. Grieser, S. Meak, J. Martha, H. H. Dewey, S. Kales, D. Berenzy, K. Carpenter-Azevedo, E. King, R. C. Huard, S. C. Smole, C. M. Brown, T. Fink, A. S. Lang, G. R. Gallagher, P. C. Sabeti, S. Gabriel, B. L. MacInnis, New England Variant Investigation Team, R. Tewhey, M. D. Adams, D. J. Park, J. E. Lemieux, N. D. Grubaugh, Comparative transmissibility of SARS-CoV-2 variants Delta and Alpha in New England, USA. medRxiv 2021.10.06.21264641 [Preprint] (2021). https://doi.org/10.1101/2021.10.06.21264641.
5. K. B. Pouwels, E. Pritchard, P. C. Matthews, N. Stoesser, D. W. Eyre, K.-D. Vihta, T. House, J. Hay, J. I. Bell, J. N. Newton, J. Farrar, D. Crook, D. Cook, E. Rourke, R. Studley, T. E. A. Peto, I. Diamond, A. S. Walker, Effect of Delta variant on viral burden and vaccine effectiveness against new SARS-CoV-2 infections in the UK. *Nat. Med.* **27**, 2127–2135 (2021). doi:10.1038/s41591-021-01548-7 Medline
6. Y. Cao, J. Wang, F. Jian, T. Xiao, W. Song, A. Yisimayi, W. Huang, Q. Li, P. Wang, R. An, J. Wang, Y. Wang, X. Niu, S. Yang, H. Liang, H. Sun, T. Li, Y. Yu, Q. Cui, S. Liu, X. Yang, S. Du, Z. Zhang, X. Hao, F. Shao, R. Jin, X. Wang, J. Xiao, Y. Wang, X. S. Xie, Omicron escapes the majority of existing SARS-CoV-2 neutralizing antibodies. *Nature* (2021). doi:10.1038/s41586-021-04385-3 Medline
7. D. Planas, N. Saunders, P. Maes, F. Guivel-Benhassine, C. Planchais, J. Buchrieser, W.-H. Bolland, F. Porrot, I. Staropoli, F. Lemoine, H. Péré, D. Veyer, J. Puech, J.

Rodary, G. Baele, S. Dellicour, J. Raymenants, S. Gorissen, C. Geenen, B. Vanmechelen, T. Wawina-Bokalanga, J. Martí-Carreras, L. Cuypers, A. Sève, L. Hocqueloux, T. Prazuck, F. Rey, E. Simon-Loriere, T. Bruel, H. Mouquet, E. André, O. Schwartz, Considerable escape of SARS-CoV-2 Omicron to antibody neutralization. *Nature* (2021). doi:10.1038/s41586-021-04389-z Medline

8. L. Liu, S. Iketani, Y. Guo, J. F.-W. Chan, M. Wang, L. Liu, Y. Luo, H. Chu, Y. Huang, M. S. Nair, J. Yu, K. K.-H. Chik, T. T.-T. Yuen, C. Yoon, K. K.-W. To, H. Chen, M. T. Yin, M. E. Sobieszczyk, Y. Huang, H. H. Wang, Z. Sheng, K.-Y. Yuen, D. D. Ho, Striking antibody evasion manifested by the Omicron variant of SARS-CoV-2. *Nature* (2021). doi:10.1038/s41586-021-04388-0 Medline
9. D. Wrapp, N. Wang, K. S. Corbett, J. A. Goldsmith, C.-L. Hsieh, O. Abiona, B. S. Graham, J. S. McLellan, Cryo-EM structure of the 2019-nCoV spike in the prefusion conformation. *Science* **367**, 1260–1263 (2020). doi:10.1126/science.abb2507 Medline
10. C. L. Hsieh, J. A. Goldsmith, J. M. Schaub, A. M. DiVenere, H.-C. Kuo, K. Javanmardi, K. C. Le, D. Wrapp, A. G. Lee, Y. Liu, C.-W. Chou, P. O. Byrne, C. K. Hjorth, N. V. Johnson, J. Ludes-Meyers, A. W. Nguyen, J. Park, N. Wang, D. Amengor, J. J. Lavinder, G. C. Ippolito, J. A. Maynard, I. J. Finkelstein, J. S. McLellan, Structure-based design of prefusion-stabilized SARS-CoV-2 spikes. *Science* **369**, 1501–1505 (2020). doi:10.1126/science.abd0826 Medline
11. E. Cameroni, J. E. Bowen, L. E. Rosen, C. Saliba, S. K. Zepeda, K. Culap, D. Pinto, L. A. VanBlargan, A. De Marco, J. di Iulio, F. Zatta, H. Kaiser, J. Noack, N. Farhat, N. Czudnochowski, C. Havenar-Daughton, K. R. Sprouse, J. R. Dillen, A. E. Powell, A. Chen, C. Maher, L. Yin, D. Sun, L. Soriaga, J. Bassi, C. Silacci-Fregni, C. Gustafsson, N. M. Franko, J. Logue, N. T. Iqbal, I. Mazzitelli, J. Geffner, R. Grifantini, H. Chu, A. Gori, A. Riva, O. Giannini, A. Ceschi, P. Ferrari, P. E. Cippà, A. Franzetti-Pellanda, C. Garzoni, P. J. Halfmann, Y. Kawaoka, C. Hebner, L. A. Purcell, L. Piccoli, M. S. Pizzuto, A. C. Walls, M. S. Diamond, A. Telenti, H. W. Virgin, A. Lanzavecchia, G. Snell, D. Veesler, D. Corti, Broadly neutralizing antibodies overcome SARS-CoV-2 Omicron antigenic shift. *Nature* (2021). doi:10.1038/s41586-021-04386-2 Medline
12. J. Juraszek, L. Rutten, S. Blokland, P. Bouchier, R. Voorzaat, T. Ritschel, M. J. G. Bakkers, L. L. R. Renault, J. P. M. Langedijk, Stabilizing the closed SARS-CoV-2 spike trimer. *Nat. Commun.* **12**, 244 (2021). doi:10.1038/s41467-020-20321-x Medline
13. X. Chi, R. Yan, J. Zhang, G. Zhang, Y. Zhang, M. Hao, Z. Zhang, P. Fan, Y. Dong, Y. Yang, Z. Chen, Y. Guo, J. Zhang, Y. Li, X. Song, Y. Chen, L. Xia, L. Fu, L. Hou, J. Xu, C. Yu, J. Li, Q. Zhou, W. Chen, A neutralizing human antibody binds to the N-terminal domain of the Spike protein of SARS-CoV-2. *Science* **369**, 650–655 (2020). doi:10.1126/science.abc6952 Medline
14. J. Hansen, A. Baum, K. E. Pascal, V. Russo, S. Giordano, E. Wloga, B. O. Fulton, Y. Yan, K. Koon, K. Patel, K. M. Chung, A. Hermann, E. Ullman, J. Cruz, A. Rafique, T. Huang, J. Fairhurst, C. Libertiny, M. Malbec, W. Y. Lee, R. Welsh, G. Farr, S. Pennington, D. Deshpande, J. Cheng, A. Watty, P. Bouffard, R. Babb, N. Levenkova, C. Chen, B. Zhang, A. Romero Hernandez, K. Saotome, Y. Zhou, M. Franklin, S. Sivapalasingam, D. C. Lye, S. Weston, J. Logue, R. Haupt, M. Frieman, G. Chen, W. Olson, A. J. Murphy, N. Stahl, G. D. Yancopoulos, C. A. Kyratsous, Studies in humanized mice and convalescent humans yield a SARS-CoV-2 antibody cocktail. *Science* **369**, 1010–1014 (2020). doi:10.1126/science.abd0827 Medline
15. B. E. Jones, P. L. Brown-Augsburger, K. S. Corbett, K. Westendorf, J. Davies, T. P. Cujec, C. M. Wiethoff, J. L. Blackbourne, B. A. Heinz, D. Foster, R. E. Higgs, D. Balasubramaniam, L. Wang, Y. Zhang, E. S. Yang, R. Bidshahri, L. Kraft, Y. Hwang, S. Žentelis, K. R. Jepson, R. Goya, M. A. Smith, D. W. Collins, S. J. Hinshaw, S. A. Tycho, D. Pellacani, P. Xiang, K. Muthuraman, S. Sobhanifar, M. H. Piper, F. J. Triana, J. Hendle, A. Pustilnik, A. C. Adams, S. J. Berens, R. S. Baric, D. R. Martinez, R. W. Cross, T. W. Geisbert, V. Borisevich, O. Abiona, H. M. Belli, M. de Vries, A. Mohamed, M. Dittmann, M. I. Samanovic, M. J. Mulligan, J. A. Goldsmith, C.-L. Hsieh, N. V. Johnson, D. Wrapp, J. S. McLellan, B. C. Barnhart, B. S. Graham, J. R. Mascola, C. L. Hansen, E. Falconer, The neutralizing antibody, LY-CoV555, protects against SARS-CoV-2 infection in nonhuman primates. *Sci. Transl. Med.* **13**, eabf1906 (2021). doi:10.1126/scitranslmed.abf1906 Medline
16. D. Pinto, Y.-J. Park, M. Beltramello, A. C. Walls, M. A. Tortorici, S. Bianchi, S. Jaconi, K. Culap, F. Zatta, A. De Marco, A. Peter, B. Guarino, R. Spreafico, E. Cameroni, J. B. Case, R. E. Chen, C. Havenar-Daughton, G. Snell, A. Telenti, H. W. Virgin, A. Lanzavecchia, M. S. Diamond, K. Fink, D. Veesler, D. Corti, Cross-neutralization of SARS-CoV-2 by a human monoclonal SARS-CoV antibody. *Nature* **583**, 290–295 (2020). doi:10.1038/s41586-020-2349-y Medline
17. Q. Wang, Y. Zhang, L. Wu, S. Niu, C. Song, Z. Zhang, G. Lu, C. Qiao, Y. Hu, K.-Y. Yuen, Q. Wang, H. Zhou, J. Yan, J. Qi, Structural and functional basis of SARS-CoV-2 entry by using human ACE2. *Cell* **181**, 894–904.e9 (2020). doi:10.1016/j.cell.2020.03.045 Medline
18. J. Lan, J. Ge, J. Yu, S. Shan, H. Zhou, S. Fan, Q. Zhang, X. Shi, Q. Wang, L. Zhang, X. Wang, Structure of the SARS-CoV-2 spike receptor-binding domain bound to the ACE2 receptor. *Nature* **581**, 215–220 (2020). doi:10.1038/s41586-020-2180-5 Medline
19. C. Toelzer, K. Gupta, S. K. N. Yadav, U. Borucu, A. D. Davidson, M. Kavanagh Williamson, D. K. Shoemark, F. Garzoni, O. Staufer, R. Milligan, J. Capin, A. J. Mulholland, J. Spatz, D. Fitzgerald, I. Berger, C. Schaffitzel, Free fatty acid binding pocket in the locked structure of SARS-CoV-2 spike protein. *Science* **370**, 725–730 (2020). doi:10.1126/science.abd3255 Medline
20. C. Gu, X. Cao, Z. Wang, X. Hu, Y. Yao, Y. Zhou, P. Liu, X. Liu, G. Gao, X. Hu, Y. Zhang, Z. Chen, L. Gao, Y. Peng, F. Jia, C. Shan, L. Yu, K. Liu, N. Li, W. Guo, G. Jiang, J. Min, J. Zhang, L. Yang, M. Shi, T. Hou, Y. Li, W. Liang, G. Lu, C. Yang, Y. Wang, K. Xia, Z. Xiao, J. Xue, X. Huang, X. Chen, H. Ma, D. Song, Z. Pan, X. Wang, H. Guo, H. Liang, Z. Yuan, W. Guan, S.-J. Deng, A human antibody of potent efficacy against SARS-CoV-2 in rhesus macaques showed strong blocking activity to B.1.351. *MAbs* **13**, 1930636 (2021). doi:10.1080/19420862.2021.1930636 Medline
21. Y. Yan, S. Mukherjee, K. G. Harikumar, T. S. Strutzenberg, X. E. Zhou, K. Suino-Powell, T.-H. Xu, R. D. Sheldon, J. Lamp, J. S. Brunzelle, K. Radziwon, A. Ellis, S. J. Novick, I. E. Vega, R. G. Jones, L. J. Miller, H. E. Xu, P. R. Griffin, A. A. Kossiakoff, K. Melcher, Structure of an AMPK complex in an inactive, ATP-bound state. *Science* **373**, 413–419 (2021). doi:10.1126/science.abe7565 Medline
22. S. Kumar, A. Chandele, A. Sharma, Current status of therapeutic monoclonal antibodies against SARS-CoV-2. *PLOS Pathog.* **17**, e1009885 (2021). doi:10.1371/journal.ppat.1009885 Medline
23. S. Q. Zheng, E. Palovcak, J.-P. Armache, K. A. Verba, Y. Cheng, D. A. Agard, MotionCor2: Anisotropic correction of beam-induced motion for improved cryo-electron microscopy. *Nat. Methods* **14**, 331–332 (2017). doi:10.1038/nmeth.4193 Medline
24. A. Rohou, N. Grigorieff, CTFFIND4: Fast and accurate defocus estimation from electron micrographs. *J. Struct. Biol.* **192**, 216–221 (2015). doi:10.1016/j.jsb.2015.08.008 Medline
25. J. Zivanov, T. Nakane, B. O. Forsberg, D. Kimanius, W. J. H. Hagen, E. Lindahl, S. H. W. Scheres, New tools for automated high-resolution cryo-EM structure determination in RELION-3. *eLife* **7**, e42166 (2018). doi:10.7554/eLife.42166 Medline
26. A. Punjani, J. L. Rubinstein, D. J. Fleet, M. A. Brubaker, cryoSPARC: Algorithms for rapid unsupervised cryo-EM structure determination. *Nat. Methods* **14**, 290–296 (2017). doi:10.1038/nmeth.4169 Medline
27. R. Sanchez-Garcia, J. Gomez-Blanco, A. Cuervo, J. M. Carazo, C. O. S. Sorzano, J. Vargas, DeepEMhancer: A deep learning solution for cryo-EM volume post-processing. *Commun. Biol.* **4**, 874 (2021). doi:10.1038/s42003-021-02399-1 Medline
28. T. Schwede, J. Kopp, N. Guex, M. C. Peitsch, SWISS-MODEL: An automated protein homology-modeling server. *Nucleic Acids Res.* **31**, 3381–3385 (2003). doi:10.1093/nar/gkg520 Medline
29. T. Zhou, Y. Tsybovsky, J. Gorman, M. Rapp, G. Cerutti, G.-Y. Chuang, P. S. Katsamba, J. M. Sampson, A. Schön, J. Bimela, J. C. Boyington, A. Nazzari, A. S. Olia, W. Shi, M. Sastry, T. Stephens, J. Stuckey, I.-T. Teng, P. Wang, S. Wang, B. Zhang, R. A. Friesner, D. D. Ho, J. R. Mascola, L. Shapiro, P. D. Kwong, Cryo-EM structures of SARS-CoV-2 Spike without and with ACE2 reveal a pH-dependent switch to mediate endosomal positioning of receptor-binding domains. *Cell Host Microbe* **28**, 867–879.e5 (2020). doi:10.1016/j.chom.2020.11.004 Medline
30. A. C. Walls, Y.-J. Park, M. A. Tortorici, A. Wall, A. T. McGuire, D. Veesler, Structure, function, and antigenicity of the SARS-CoV-2 Spike glycoprotein. *Cell* **181**, 281–292.e6 (2020). doi:10.1016/j.cell.2020.02.058 Medline
31. E. F. Pettersen, T. D. Goddard, C. C. Huang, G. S. Couch, D. M. Greenblatt, E. C. Meng, T. E. Ferrin, UCSF Chimera--A visualization system for exploratory research and analysis. *J. Comput. Chem.* **25**, 1605–1612 (2004). doi:10.1002/jcc.20084 Medline
32. P. Emsley, K. Cowtan, Coot: Model-building tools for molecular graphics. *Acta Crystallogr. D Biol. Crystallogr.* **60**, 2126–2132 (2004). doi:10.1107/S0907444904019158 Medline
33. P. D. Adams, K. Gopal, R. W. Grosse-Kunstleve, L.-W. Hung, T. R. Ioerger, A. J.

McCoy, N. W. Moriarty, R. K. Pai, R. J. Read, T. D. Romo, J. C. Sacchettini, N. K. Sauter, L. C. Storoni, T. C. Terwilliger, Recent developments in the PHENIX software for automated crystallographic structure determination. *J. Synchrotron Radiat.* **11**, 53–55 (2004). doi:10.1107/S0909049503024130 Medline

34. T. I. Croll, ISOLDE: A physically realistic environment for model building into low-resolution electron-density maps. *Acta Crystallogr. D Struct. Biol.* **74**, 519–530 (2018). doi:10.1107/S2059798318002425 Medline
35. E. F. Pettersen, T. D. Goddard, C. C. Huang, E. C. Meng, G. S. Couch, T. I. Croll, J. H. Morris, T. E. Ferrin, UCSF ChimeraX: Structure visualization for researchers, educators, and developers. *Protein Sci.* **30**, 70–82 (2021). doi:10.1002/pro.3943 Medline
36. K. Melcher, L.-M. Ng, X. E. Zhou, F.-F. Soon, Y. Xu, K. M. Suino-Powell, S.-Y. Park, J. J. Weiner, H. Fujii, V. Chinnusamy, A. Kovach, J. Li, Y. Wang, J. Li, F. C. Peterson, D. R. Jensen, E.-L. Yong, B. F. Volkman, S. R. Cutler, J.-K. Zhu, H. E. Xu, A gate-latch-lock mechanism for hormone signalling by abscisic acid receptors. *Nature* **462**, 602–608 (2009). doi:10.1038/nature08613 Medline

ACKNOWLEDGMENTS

The cryo-EM data were collected at the Shanghai Advanced Electron Microscope Center. **Funding**: This work was partially supported by Ministry of Science and Technology (China) grants (2018YFA0507002 to H.E.X.); Shanghai Municipal Science and Technology Major Project (2019SHZDZX02 to H.E.X.); Shanghai Municipal Science and Technology Major Project (H.E.X.); CAS Strategic Priority Research Program (XDB37030103 to H.E.X.), National Natural Science Foundation of China (32130022 to H.E.X.); the Youth Innovation Promotion Association of CAS (2021278 to W.Y.), National Natural Science Foundation of China (32171189 to W.Y.), National Science Fund for Excellent Young Scholars (82122067 to W.Y.), Key tasks of LG laboratory (LG202103-03-05 to W.Y.); Fund of Youth Innovation Promotion Association (2018319 Y8G7011009 to X.C.); Science and Technology Commission of Shanghai Municipal (20431900100 to H.J.) and Jack Ma Foundation (2020-CMKYGG-05 to H.J.); National Natural Science Foundation (31770796 to Y.J.) and National Science and Technology Major Project (2018ZX09711002 to Y.J.); National Natural Science Foundation of China (81902085 to Y.X.); Shanghai Municipal Science and Technology Major Project (to J. Z.). China Postdoctoral Science Foundation Funded Project (Project No.E11289R078 to C.W.); Key tasks of LG laboratory (LG202101- 01-03 to Y. X.). **Author contributions**: W.Y. designed the expression constructs, purified the Spike complex proteins, screened the cryo-EM conditions, prepared the cryo-EM grids and collected cryo-EM images toward the structures, and participated in figure and manuscript preparation. Y.X. collected cryo-EM images with the help of Q.Y., K.W. and W.H, performed density map calculations and participated in the model building and refined the final models with P.X., Y.X., P.X. and C.W. participated in figure and manuscript preparation. X.W. purified the ACE2 protein. S.H. performed the AlphaScreen assays. H.J. supervised X.C., Z.H. and X.H., analyzed the molecular 13 dynamics simulations and participated in figure preparation. J. Z. supervised B.S., detected the HDX data by mass spectrometry and participated in figure preparation; Y.J. participated in experimental design and manuscript editing. S. D. supervised X.C., C.G., J.L., Z.W., F.J., K.X., P.L., and X.W., provided the JMB2002 antibodies, performed the function assays for JMB2002 antibodies and spike proteins, and participated in manuscript writing; H.E.X. conceived and supervised the project, analyzed the structures, and wrote the manuscript with inputs from all authors. **Competing interests**: Wanchao Yin, Youwei Xu, Peiyu Xu, Canrong Wu, Xinheng He, Xiaoxi Wang, Sijie Huang, Qingning Yuan, Kai Wu, Wen Hu, Zifu Huang, Bin Song, Jie Zheng, Hualiang Jiang, Xi Cheng, Yi Jiang, H. Eric Xu have declared no competing interest. Xiaodan Cao, Chunyin Gu, Jia Liu, Zongda Wang, Fangfang Jia, Kaiwen Xia, Peipei Liu, Xueping Wang, and Su-Jun Deng are employee of Shanghai Jemincare Pharmaceuticals, and are developing JMB2002 as a potential anti-Omicron therapeutic. **Data and materials availability**: Density maps and structure coordinates have been deposited with immediate release. The accession numbers of Electron Microscopy Database and the Protein Data Bank are EMD-32679 and PDB ID 7WP9 for Omicron spike trimer; EMD-32680 and PDB ID 7WPA for Omicron spike trimer in complex with hACE2; EMD-32681 and PDB ID 7WPB for local refined reconstruction of Omicron spike RBD in complex with hACE2; EMD-32682 and PDB ID 7WPC for local refined reconstruction of a second Omicron spike RBD in complex with RBD-hACE2; EMD-32683 and PDB ID 7WPD for Omicron spike trimer in complex with one JMB2002 Fab; EMD-32684 and PDB ID 7WPE for Omicron spike trimer in complex with two JMB2002 Fab; EMD-32685 and PDB ID 7WPF for Omicron spike trimer in complex with three JMB2002 Fab, EMD-32736 and PDB ID 7WRV for local refined reconstruction of Omicron spike RBD in complex with JMB2002 Fab. Materials are available upon request.

SUPPLEMENTARY MATERIALS

science.org/doi/10.1126/science.abn8863
Materials and Methods
Figs. S1 to S10
Tables S1 and S3
References (*23*–*36*)
Table S2
MDAR Reproducibility Checklist

27 December 2021; accepted 2 February 2022
Published online 8 February 2022
10.1126/science.abn8863

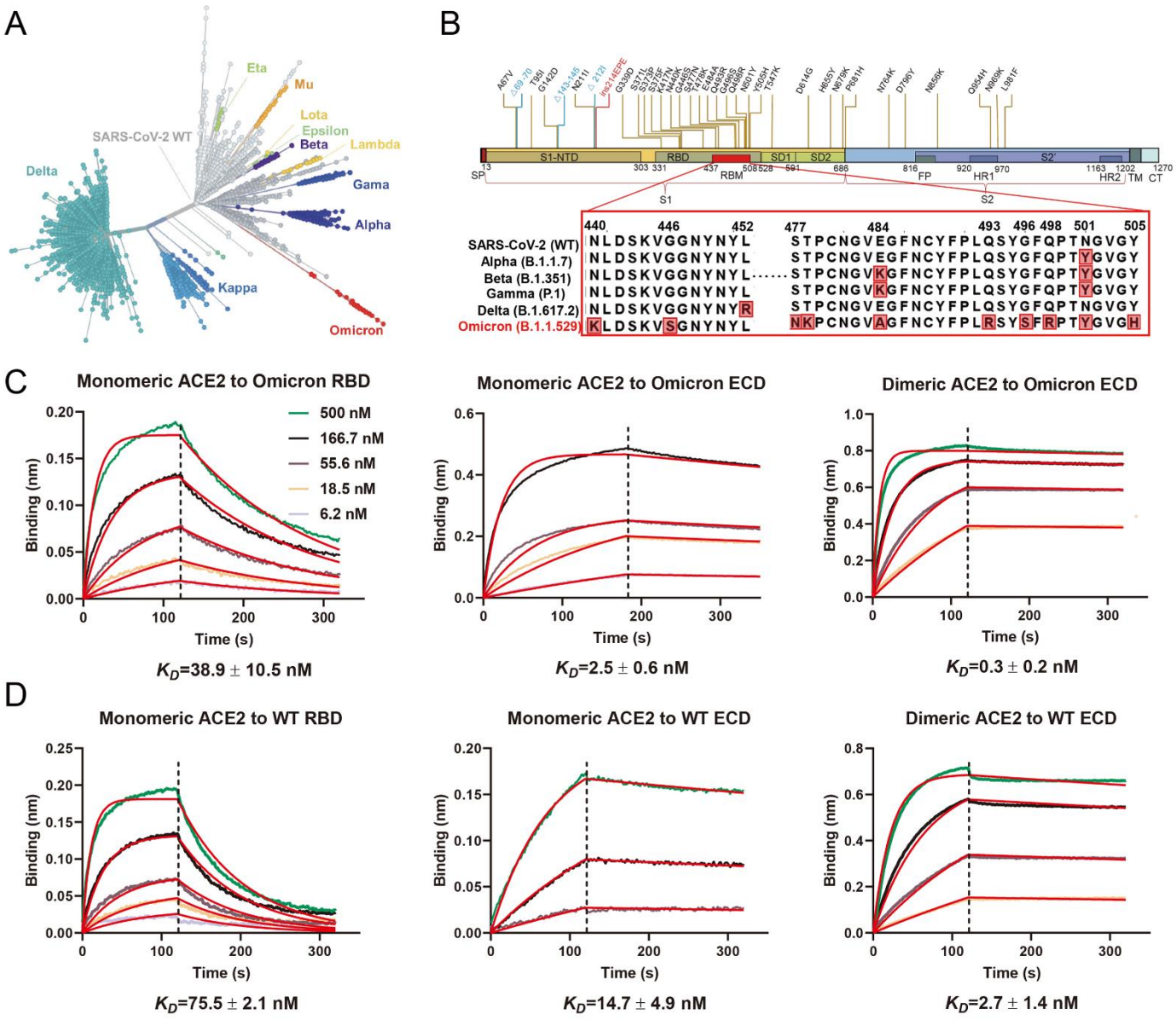

Fig. 1. High-affinity binding of the SARS-CoV-2 Omicron spike protein with human ACE2. (**A**) Phylogeny of the SARS-CoV-2 variants. Variants of concern and variants of interest are labeled on the graph, the number of spike protein mutations are positively correlated with the distance from the original strain. (**B**) Schematic of Omicron spike protein domain architecture. The mutations of Omicron spike protein are labeled with different colors (blue for deleting mutation, red for inserting mutation). Mutations in RBM are compared with wildtype SARS-CoV-2 and four other variants of concern strains. SP, signal peptide; RBD, receptor binding domain; RBM, receptor binding motif; SD1, subdomain 1; SD2, subdomain 2; FP, fusion peptide; HR1, heptad repeat 1; HR2, heptad repeat 2; TM, transmembrane region; CT, cytoplasmic tail. (**C** and **D**) Binding of Omicron and WT spike trimer and RBD to ACE2 determined by BLI.

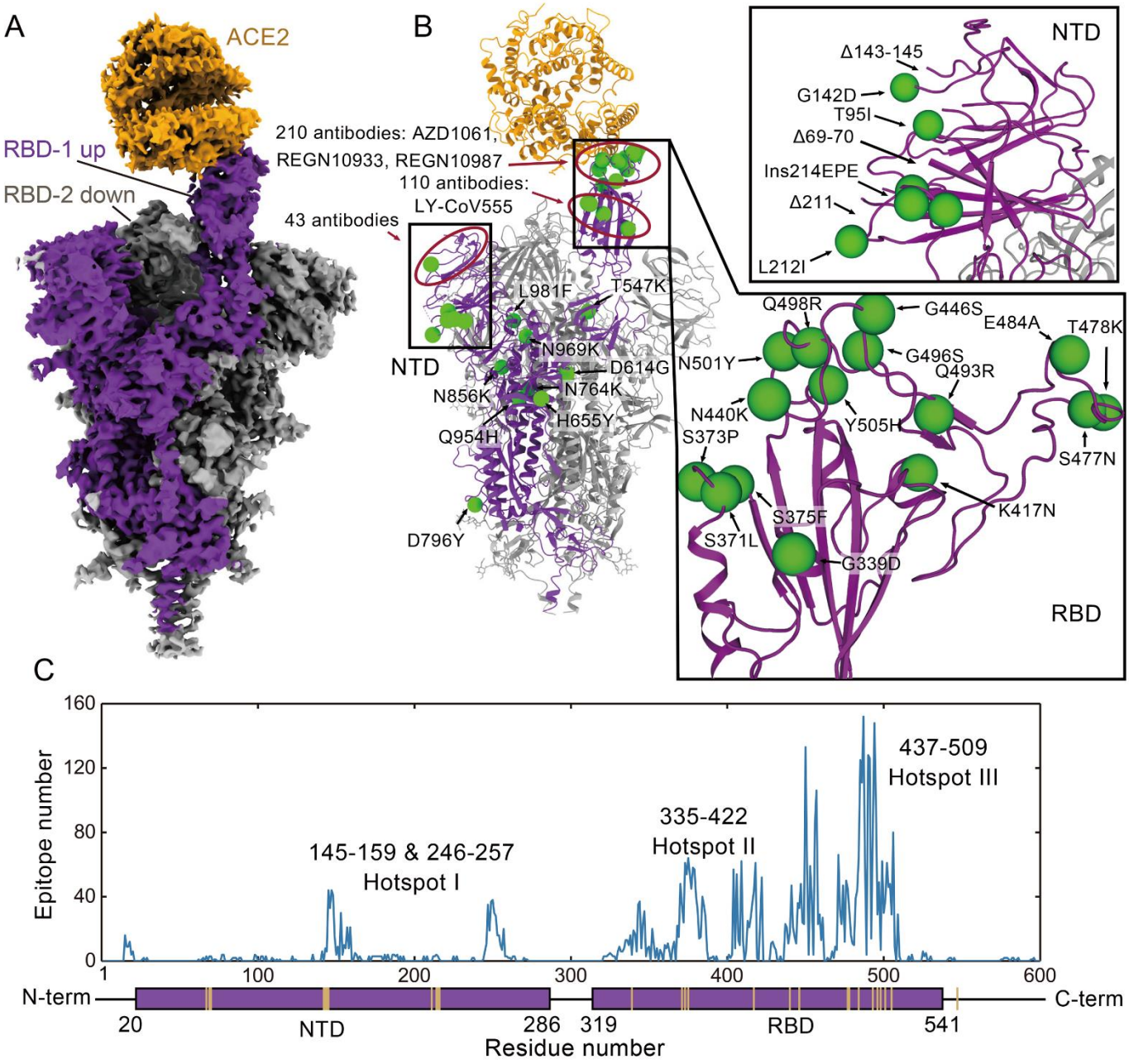

Fig. 2. The structure of ACE2 bound Omicron spike trimer complex and epitopes of current antibodies. (A) Cryo-EM density of the ACE2-Omicron spike trimer complex. (B) The overall structure of the ACE2-Omicron spike trimer complex and the locations of Omicron mutations. Epitope hotspots are highlighted in red circles with the number of antibodies indicated next to the epitopes. (C) The histogram of epitope corresponding with residue numbers. Each epitope was counted if more than 3 heavy atoms of this residue are closer than 5 Å with the antibody. The PDB IDs and corresponding epitopes were summarized in table S2 in the supplementary materials.

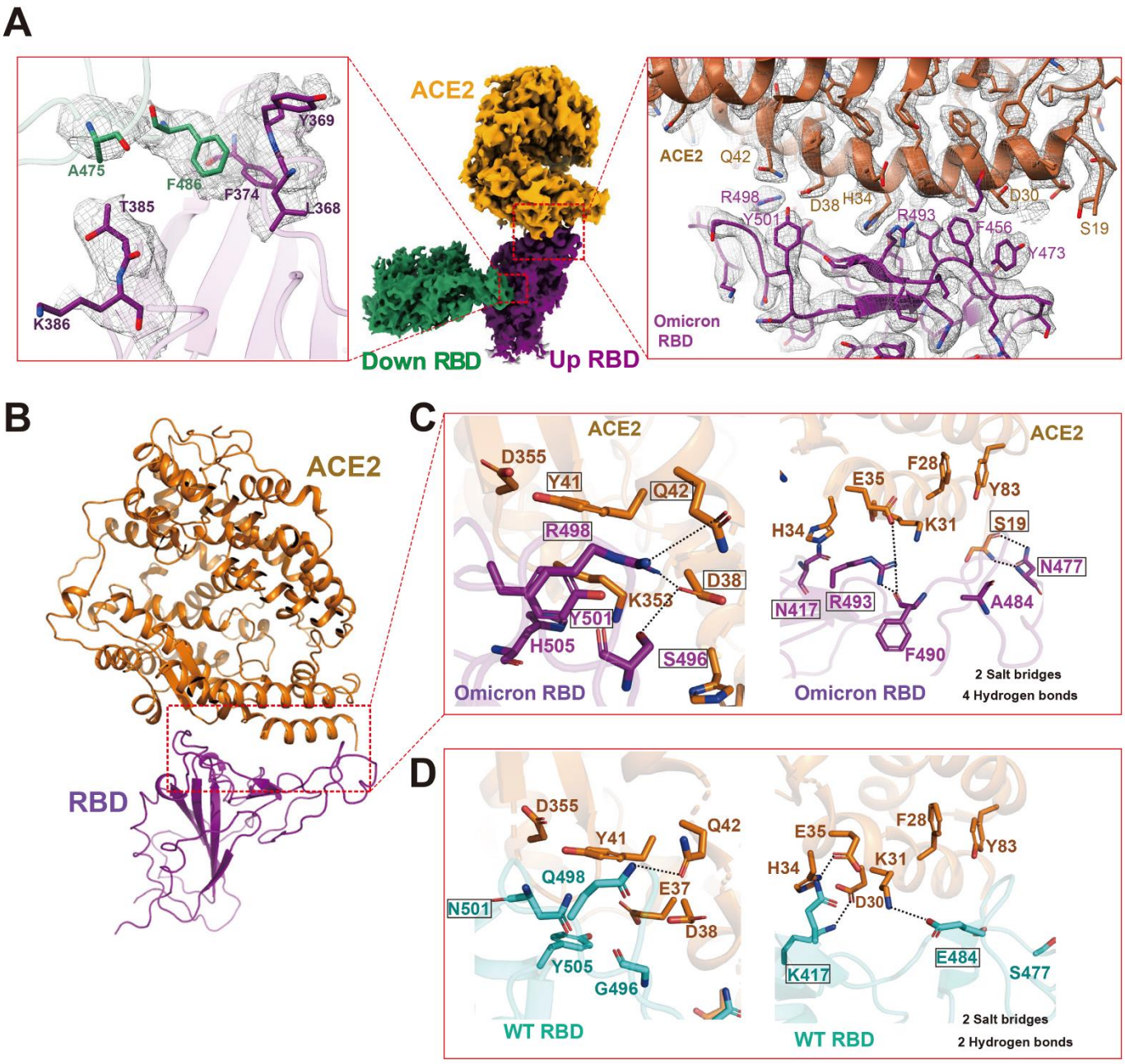

Fig. 3. Structural analysis of Omicron RBD and ACE2. (**A**) Cryo-EM density of Omicron RBD-RBD-ACE2 interface. ACE2 is colored in orange. The ACE2 bound RBD, also named up RBD is in purple. The down RBD, which directly binds to up RBD is in green. Left panel, a close-up view of RBD-RBD interaction. Middle panel, overall cryo-EM density of down RBD-RBD-ACE2 region. Right panel, the ACE2-RBD binding interface. Residues are shown in sticks with the correspondent cryo-EM density represented in mesh. (**B**) An overall structural model of Omicron RBD-ACE2 bound region. (**C**) Zoomed-in view of Omicron RBD-ACE2 with hydrogen bonds interactions. (**D**) Detailed hydrogen bonds interactions in WT RBD-ACE2 interfaces with the same view as in panel B. WT RBD is sea blue, Omicron RBD is purple, and ACE2 is orange. Hydrogen bond or salt bridge interactions are in dotted lines.

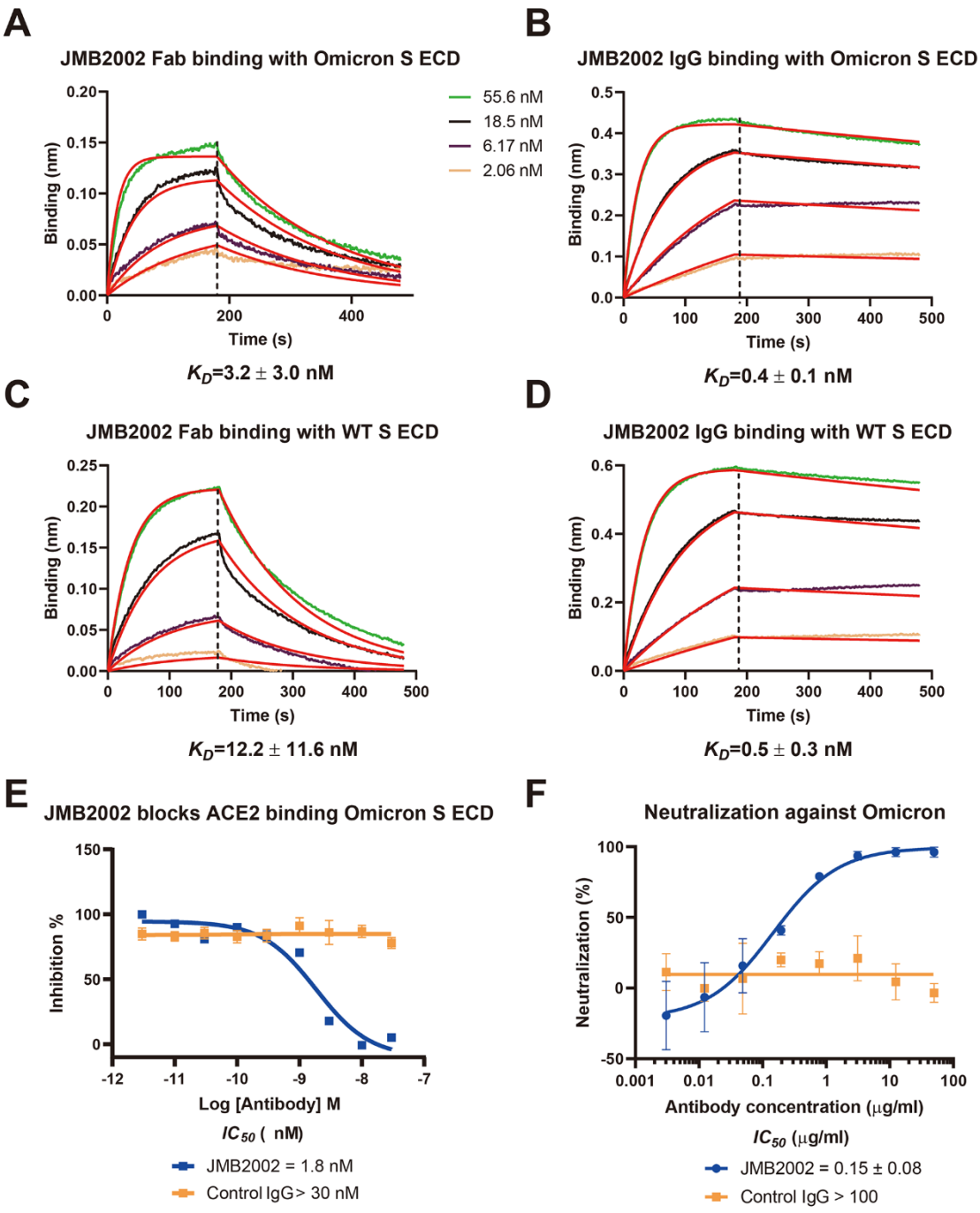

Fig. 4. Inhibition of ACE2 binding to the spike trimer by an anti-Omicron antibody. (A and C) Binding of JMB2002 Fab to Omicron and WT spike trimer. (B and D) Binding of JMB2002 IgG to Omicron and WT spike trimer. (E) Direct inhibition of ACE2 binding to the Omicron spike trimer by JMB2002. (F) Inhibition of the pseudo virus of Omicron by JMB2002.

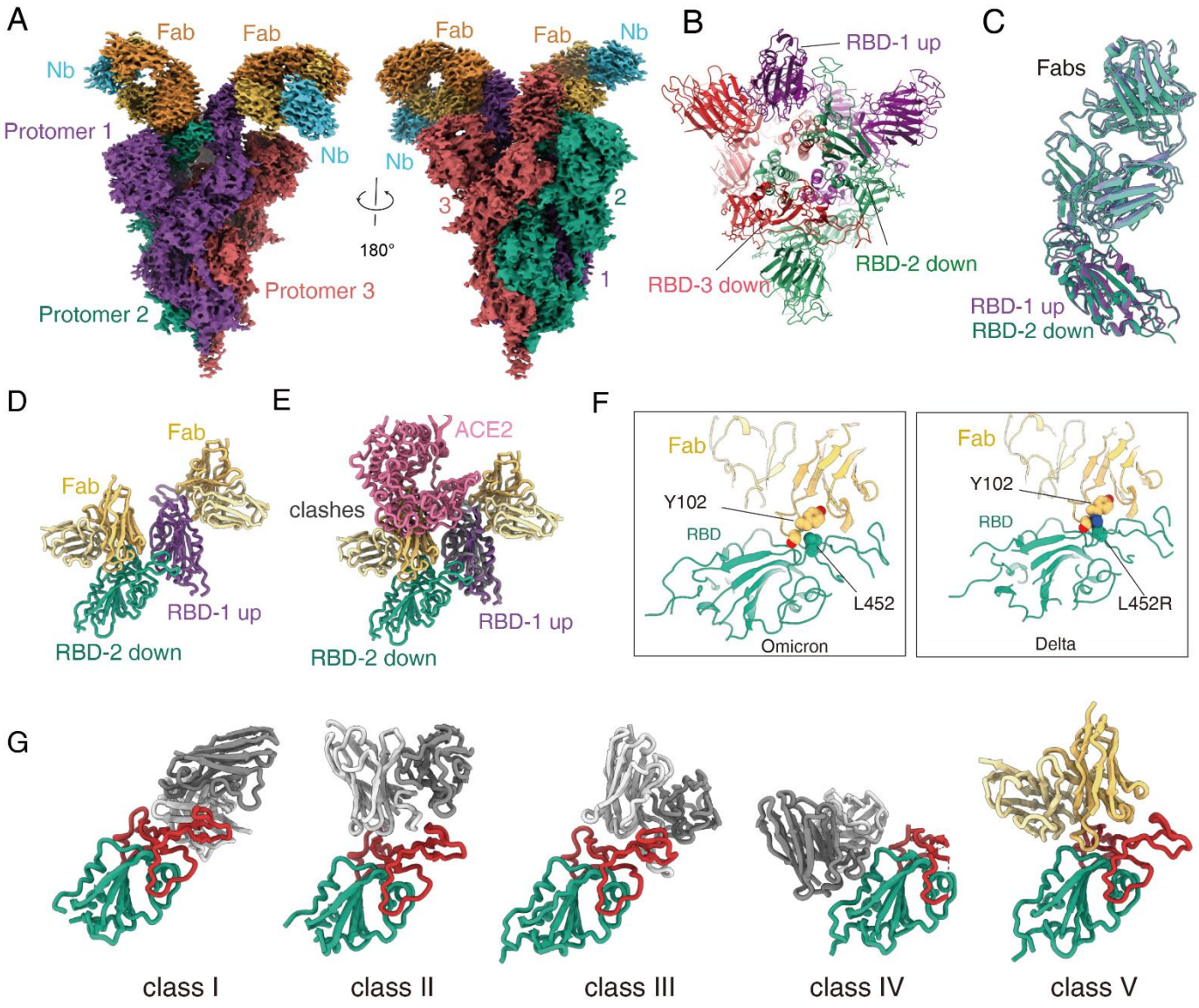

Fig. 5. Structure of Omicron spike trimer with antibody JMB2002. (A) Cryo-EM density map of the Fab-bound Omicron spike trimer showed with two front views. (B) Top view of Fab-bound Omicron spike trimer complex model with fab and nanobody hidden. (C) Superposition of the Fab bound RBD-1 and RBD-2. (D) The structure of the Fab bound RBD-1 and RBD-2. (E) Superposition of the ACE2-bound and Fab-bound RBD-1 shows the Fab binding to RBD-2 inhibits ACE2 binding to RBD-1. (F) Left panel, L452 residue from Omicron RBD interacts with Fab. Right panel, the Delta variant L452R mutation clashes the Fab binding. (G) Binding modes of 4 representative 4 classes of antibody that neutralize SARS-CoV-2. PDB codes: class I, 7CM4; class II, 7CHF; class III, 7K90; class IV, 6WPS. The JMB2002Fab in the Omicron S protein structure shows distinct binding modes from other 4 classes of antibodies.

Structures of the Omicron Spike trimer with ACE2 and an anti-Omicron antibody

Wanchao YinYouwei XuPeiyu XuXiaodan CaoCanrong WuChunyin GuXinheng HeXiaoxi WangSijie HuangQingning YuanKai WuWen HuZifu HuangJia LiuZongda WangFangfang JiaKaiwen XiaPeipei LiuXueping WangBin SongJie ZhengHualiang JiangXi ChengYi JiangSu-Jun DengH. Eric Xu

Science, **Ahead of Print** • DOI: 10.1126/science.abn8863